Interdependence of Profilin, Cation, and Nucleotide Binding to Vertebrate Non-Muscle Actin†

Henry J. Kinosian,*,‡ Lynn A. Selden,§ Lewis C. Gershman,§,|| and James E. Estes‡,§

Center for Molecular Biology and Cancer Research and Department of Medicine, Albany Medical College, Albany, New York 12208, and Research Service and Medical Service, Department of Veterans Affairs Samuel S. Stratton Medical Center, Albany, New York 12208

Received July 5, 2000

ABSTRACT: The interaction of profilin and non-muscle β,γ-actin prepared from bovine spleen has been investigated under physiologic ionic conditions. Profilin binding to actin decreases the affinity of actin for MgADP and MgATP by about 65- and 13-fold, respectively. Kinetic measurements indicate that profilin binding to actin weakens the affinity of actin for nucleotides primarily due to an increased nucleotide dissociation rate constant, but the nucleotide association rate constant is also increased about 2-fold. Removal of the actin-bound nucleotide and divalent cation produces the labile intermediate species in the nucleotide exchange reaction, nucleotide free actin (NF-actin), and increases the affinity of actin for profilin about 10-fold. Profilin binds NF-actin with high affinity, $K_D = 0.013\ \mu M$, and slows the observed denaturation rate of NF-actin. Addition of ATP to NF-actin weakens the affinity for profilin and addition of Mg^{2+} to ATP-actin further weakens the affinity for profilin. The high-affinity Mg^{2+} of actin regulates binding of both nucleotide and profilin to actin and is important for actin interdomain coupling. The data suggest that profilin binding to actin weakens nucleotide binding to actin by disrupting Mg^{2+} coordination in the actin central cleft.

Actin and profilin are ubiquitous vertebrate proteins found intracellularly in high concentrations. Profilin is thought to play important roles in signal pathways and control of cellular cytoskeletal changes via interactions with proteins and lipids (for review see ref *1*). Profilin binding by actin has been shown to increase the rate of nucleotide exchange on monomeric actin (*2*−*5*). It is thought that profilin functions in vivo to promote actin polymerization from a sequestered pool of monomeric actin bound to thymosin-β_4 (*6*, *7*) and profilin−actin interacts with WASP/Scar proteins to elongate actin filament barbed ends (*8*). Overexpression of profilin by Chinese hamster ovary cells leads to increases in F-actin concentration and actin filament half-life (*9*). This observation is in concert with the report that in vitro in the presence of high number concentrations of actin filaments, profilin decreases the steady-state concentration of monomer MgADPactin[1] and increases the steady-state F-actin concentration by increasing the nucleotide exchange rate (*3*). It has been proposed that profilin promotes the formation of actin filaments formed from a homogeneous population of MgATPactin which after polymerization hydrolyze ATP to transiently produce F-actin containing bound MgADP and inorganic phosphate (P_i) (*3*). The dissociation of P_i from the actin filament is thought to be a limiting step for the binding of ADF/cofilin (*10*), Arp2/3 complex (*8*) and subsequent rapid actin depolymerization (*11*). Moreover, because DNase I, thymosin-β_4, and cofilin inhibit nucleotide exchange on actin, profilin may be necessary for adequate nucleotide exchange on actin in the presence of these intracellular proteins.

To our knowledge, the interaction of profilin with non-muscle vertebrate actin in its physiological MgATP and MgADP containing forms and in the presence of physiological salt concentrations has not been previously investigated. It has been previously reported that actin and profilin from different sources have different binding affinities and function differently; for example, some plant profilins do not increase actin-bound nucleotide exchange (*12*). We find that compared to what has been previously reported for α-skeletal muscle actin (*3*, *13*), non-muscle β,γ-actin binds nucleotides with lower affinity and binds profilin with a higher affinity. This

† This work was supported by Department of Veterans Affairs Grant 1912-0001 (J.E.E.).

* To whom correspondence should be addressed. Phone: (518) 462-3311, ext. 2213. Fax: (518) 462-0626. E-mail: henry.kinosian@med.va.gov.

‡ Center for Molecular Biology and Cancer Research, Albany Medical College.

§ Research Service, Department of Veterans Affairs Samuel S. Stratton Medical Center, and Department of Medicine, Albany Medical College.

|| Department of Medicine, Albany Medical College, and Medical Service, Department of Veterans Affairs Samuel S. Stratton Medical Center.

[1] Abbreviations: MgATPactin and MgADPactin indicate monomeric actin which contains bound MgATP and MgADP, respectively; DCF-ATPactin, divalent cation free actin which contains bound ATP but no divalent cation; NF-actin, nucleotide free actin which contains neither nucleotide nor divalent cation; profilin−actin, the noncovalent binary complex of profilin and actin (the actin-bound nucleotide is unspecified); ϵATP, 1,N^6-etheno-adenosine 5′-triphosphate; ϵADP, 1,N^6-etheno-adenosine 5′-diphosphate; EGTA, ethylene glycol-bis(β-aminoethyl ether) *N*,*N*,*N*′,*N*′-tetraacetic acid; MOPS, 3-[morpholino]propanesulfonic acid.

10.1021/bi001520+ CCC: $19.00
Published on Web 10/03/2000

means that compared to skeletal muscle actin, non-muscle actin exchanges bound nucleotide faster and that profilin more effectively enhances the rate of nucleotide exchange on non-muscle actin. Teleologically, it appears that non-muscle β,γ-actin is well suited for rapid actin monomer cycling that is known to take place in motile cells.

Profilin-actin crystal structures demonstrate that the actin nucleotide binding cleft opens and closes as the two major actin domains move relative to each other via shear motions involving residues that are part of an interdomain helix (*14*, *15*). In the open state of actin, the nucleotide is much more solvent accessible and the divalent cation coordination with protein residues in the cleft is disrupted. The profilin binding site is located at the actin "barbed" end between the two major actin domains and at the opposite side of the interdomain helix from the nucleotide binding cleft (*14*, *16*). It has been suggested that binding of profilin by actin fixes the actin interdomain angle (*17*).

In the present report, we characterize the interaction of profilin and nucleotides with β,γ-actin under physiologic ionic conditions. Profilin catalyzes nucleotide exchange for the physiologically relevant MgADPactin form of actin by increasing the MgADP dissociation rate constant by about 2 orders of magnitude. In contrast, profilin has little effect on the rate constant for dissociation of ATP from DCF-ATPactin. The data suggest that profilin binding to actin weakens the nucleotide affinity primarily by disruption of the Mg^{2+} coordination by residues in the actin cleft. Conversely, MgADP or MgATP binding to actin weakens profilin affinity compared to NF-actin. NF-actin is the labile intermediate species for the exchange of nucleotides on actin and undergoes spontaneous irreversible denaturation; profilin binding stabilizes NF-actin against denaturation. The stabilization of NF-actin by profilin supports the idea that profilin compensates for the actin interdomain coupling that is lost in the absence of MgADP and MgATP.

MATERIALS AND METHODS

Protein Preparation. Non-muscle actin and profilin were purified from bovine spleen by previously published procedures (*3*, *18*). Briefly, clarified calf spleen homogenate was applied to a 5 × 8 cm poly(L-proline) column (*19*) and actin was eluted with buffer containing 0.5 M KI (*20*). After washing with 4 M urea, profilin was eluted with 8 M urea (*21*). Profilin was concentrated by application on a CM Sepharose FF column at pH 6.0 and elution with buffer containing 0.5 M KCl, pH 8.0 (*3*), and then dialyzed against 10 mM Tris, 0.5 mM DTT, pH 8.0, and stored at 4 °C until used. MgATPactin was prepared from CaATPactin by incubation with 0.3 mM EGTA and 0.3 mM $MgCl_2$ to exchange the high affinity divalent cation. MgADPactin was prepared from MgATPactin as previously described (*22*) by incubation on ice for 1 h with 10 units/mL hexokinase, 1 mM glucose, pH 8.0, then brought to pH 7.0 before use. NF-actin was prepared in the presence of ~50% sucrose by two methods, one employing Dowex AG 1 ion-exchange resin and EDTA (*23*) and another using apyrase (*24*) to remove bound ATP from actin. For experiments that measured the equilibrium dissociation constant for MgϵATP and MgϵADP to actin (Figure 4), the AG 1/EDTA method was used, because even after apyrase was diluted 20-fold, it was found to enzymatically destroy ϵATP and ϵADP within minutes. The apyrase method for NF-actin preparation was used in rapid stopped flow kinetic experiments. NF-actin in 50% sucrose was diluted 20−100-fold with buffer to a final concentration of 0.5−2.5% sucrose, so that the effect of sucrose on solution viscosity was minimal; for example, at 20 °C the viscosities of solutions of 50% and 5% sucrose are 15.4 and 1.14 cp, respectively (*25*), and the viscosity of water is 1.002 cp (*26*).

Fluorescence Measurements. Fluorescence measurements were done using an Aminco Bowman Series 2 Luminescence Spectrometer, Spectronic Instruments, Inc. For profilin titration experiments, tryptophan fluorescence intensity was measured with excitation and emission wavelengths of 300 and 335 nm, respectively. For actin denaturation experiments, tryptophan fluorescence intensity was measured with excitation and emission wavelengths of 300 and 320 nm, respectively. The ϵATP fluorescence intensity was measured with excitation and emission wavelengths of 344 and 410 nm, respectively. Kinetic measurements used a Hi-Tech SFA-11 stopped flow reactor and 1:1 volume mixing.

Actin Denaturation Experiments. As background for actin denaturation experiments in the presence of profilin and 100 mM KCl, the affinity of ATP for DCF-actin in low ionic strength buffer was determined. Actin (~40 μM) was preincubated for ~2 min with 2 mM EDTA, 2 mM Tris, 0.5 mM DTT, 0.2 mM ATP, 0.2 mM $CaCl_2$, pH 7.8, then diluted to 0.1 μM in 10 mM MOPS, pH 7.0, 2 mM EDTA, and various ATP concentrations. The tryptophan fluorescence time course was recorded and fit by a single-exponential function to yield an observed denaturation rate constant, k_{obs} (*13*). Data were fit by equation

$$k_{obs} = k_{den}/(1 + [ATP]/K_{ATP})$$

where k_{den} is the denaturation rate constant for actin without bound nucleotide and K_{ATP} is the equilibrium dissociation constant for ATP and actin. The equilibrium dissociation constants for ATP and ϵATP binding to β,γ-actin are K_{ATP} = 2.8 μM and $K_{\epsilon ATP}$ = 7.0 μM, respectively (data not shown). Addition of KCl weakens the affinity of actin for nucleotides severalfold (*2*).

For experiments depicted in Figure 1 the actin was pretreated with AG 1 anion-exchange resin to remove unbound ATP, and then added to buffer containing 10 mM MOPS, 2 mM EDTA, pH 7.0, to remove the bound Ca^{2+} and initiate denaturation. The removal of the high affinity Ca^{2+} from spleen β,γ-actin is relatively rapid ($\tau \approx 10$ s, data not shown). The denaturation rate measured here is that for NF-actin because the concentration of ATP is far below the K_{ATP} for the DCF-actin.

Titrations of Actin with Profilin. Aliquots of profilin were added to actin solutions and the tryptophan fluorescence intensity recorded. Binding of profilin by actin results in quenching of the actin fluorescence intensity (*27*). The equilibrium dissociation constant for profilin and actin was determined from a global fit to a family of observed fluorescence intensity curves using data from several total actin concentrations. The concentration of the profilin−actin complex, PA, is calculated from the total actin, A_{tot}, total profilin, P_{tot}, concentrations, and equilibrium dissociation

constant K_P, by a quadratic binding equation:

$$[PA] = \frac{[A_{tot}] + [P_{tot}] + K_P - \sqrt{([A_{tot}] + [P_{tot}] + K_P)^2 - 4[A_{tot}][P_{tot}]}}{2} \quad (1)$$

The unbound actin, A, and profilin, P, concentrations are described by

$$A = A_{tot} - PA \text{ and } P = P_{tot} - PA \quad (2)$$

The observed fluorescence, F_{obs}, is the sum of the fluorescence intensities of three protein species plus a background value, F_b, due to light scattering from the buffer alone:

$$F_{obs} = F_a[A] + F_p[P] + F_{pa}[PA] + F_b$$

where F_a, F_p, and F_{pa} are the respective specific fluorescence yields for actin, profilin, and profilin−actin, respectively. Substituting for A and P,

$$F_{obs} = F_a[A_{tot}] + F_p[P_{tot}] + (F_{pa} - F_a - F_p)[PA] + F_b$$

The fluorescence quenching due to profilin binding to actin, *Q*, is calculated:

$$Q = F_a[A_{tot}] + F_p[P_{tot}] - (F_{obs} - F_b)$$

For all titrations, the volumes of the added aliquots were recorded and the concentrations of actin and profilin were adjusted for dilution for each F_{obs} value.

Nucleotide Equilibrium Binding Measurements. Aliquots of MgϵATP or MgϵADP were added to various concentrations of NF-actin and profilin-NF-actin. The amount of actin-bound nucleotide (ϵA) can be described by

$$[\epsilon A] = \frac{[A_{tot}] + [\epsilon_{tot}] + K_\epsilon - \sqrt{([A_{tot}] + [\epsilon_{tot}] + K_\epsilon)^2 - 4[A_{tot}][\epsilon_{tot}]}}{2}$$

where A_{tot} and ϵ_{tot} are the total concentrations of actin and MgϵAXP, respectively, and K_ϵ is the equilibrium dissociation constant for nucleotide binding to actin. The observed fluorescence intensity is the sum of the fluorescence contributions of the free and bound etheno-nucleotide analogues:

$$F_{obs} = F_{\epsilon A}[\epsilon A] + F_\epsilon[\epsilon_{tot} - \epsilon A] = (F_{\epsilon A} - F_\epsilon)[\epsilon A] + F_\epsilon[\epsilon_{tot}]$$

where F_ϵ and $F_{\epsilon A}$ are the specific fluorescence yields for the free (ϵ) and bound (ϵA) forms of the etheno-nucleotides, respectively. F_{obs} values were fit to yield values for K_ϵ, $F_{\epsilon A}$, and F_ϵ. The increase in fluorescence intensity above that in the absence of actin, $\Delta\phi$, is described by

$$\Delta\phi = (F_{\epsilon A} - F_\epsilon)[\epsilon A]$$

and is proportional to the amount of bound nucleotide and is represented in Figure 4.

Nucleotide Association Kinetic Measurements. NF-actin was prepared using the apyrase method (*24*) and reacted with a 5-fold molar excess of profilin in a stopped flow reactor in buffer containing 100 mM KCl, 10 mM MOPS, and 2 mM EDTA, pH 7.0, 20 °C. To validate the pseudo-first-order analysis, differential equations were used to model second-order reaction kinetics and it was found that the pseudo-first-order kinetics described the data within experimental error.

Nucleotide Dissociation Kinetic Measurements. The time course of the fluorescence intensity increase of ϵATP upon binding to actin was measured to determine nucleotide exchange kinetics. Under the conditions used in these experiments, [ϵATP]/[ATP] = 10 or [ϵATP]/[ADP] = 10; therefore, the rate constant observed for ϵATP binding is limited by and reflects the dissociation rate constant for ATP or ADP release from actin (*13*). For MgATPactin stopped-flow experiments, one syringe contained 0.1 μM actin, 0.6 μM ATP, 100 mM KCl, 10 mM MOPS, 2 mM $MgCl_2$, pH 7.0, 20 °C (KM-buffer), and the other syringe contained 6 μM ϵATP and 2 × [profilin] in KM-buffer. In stopped flow experiments with MgADPactin, one syringe contained 2 μM actin and 12 μM ADP in KM-buffer and the other syringe contained 120 μM ϵATP and 2 × [profilin] in KM-buffer.

For experiments measuring the dissociation rate of MgATP from profilin−actin, the binding of profilin to MgATPactin can be considered to be a rapid preequilibrium (*2*), so that the observed rate constant for nucleotide exchange is described by the equation

$$k_{obs} = \frac{k_{-MgATP}[A] + k^p_{-MgATP}[PA]}{[A_{tot}]}$$

The concentrations of [PA] and [A] are calculated from a quadratic binding equation (eqs 1 and 2 above), k_{-MgATP} is the dissociation rate constant for MgATP from actin, k^p_{-MgATP} is the dissociation rate constant for MgATP from profilin−actin.

RESULTS

Profilin Stabilizes Actin against Denaturation. NF-actin is the obligate intermediate species for nucleotide exchange reactions. For some of the experiments that measure the affinity of profilin for NF-actin as well as the affinities of actin and profilin−actin for nucleotides, NF-actin must be prepared and used. Thus, it is important to know the rate at which NF-actin denatures under the ionic conditions used for the experiments described here. The decrease in tryptophan fluorescence intensity was used to measure actin denaturation (*28*, *29*). Figure 1 shows time courses for denaturation of 0.1 μM β,γ-actin in the presence and absence of 2 μM profilin and at various salt conditions. In low ionic strength buffer (circles), the denaturation time constant for NF-actin, τ_{den} = 80 (±2) s. After the rapid fluorescence decrease reflecting the initial actin unfolding, the actin goes through a subsequent slower fluorescence increase that is due to protein aggregation (*30*, *31*). Addition of 2 μM profilin to NF-actin in low ionic strength buffer (triangles) stabilizes NF-actin against denaturation and increases the denaturation time constant to τ_{den} = 395 (±11) s. NF-actin is also stabilized by the presence of 100 mM KCl in the absence of profilin, τ_{den} = 771 (±11) s (for clarity, data not shown). In the presence of both 100 mM KCl and 2 μM profilin (squares) NF-actin is further stabilized, τ_{den} = 3273 (±239) s. A control curve for 100 mM KCl, 2 mM $MgCl_2$, and 0.2

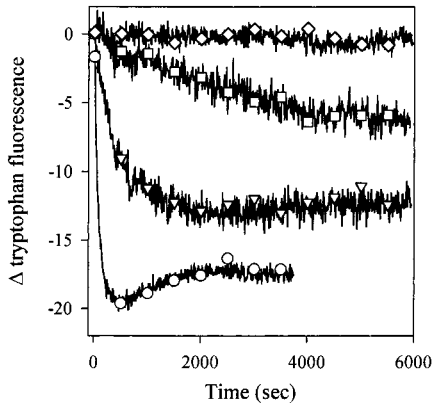

FIGURE 1: Time course data for isothermal denaturation of β,γ-NF-actin measured by actin tryptophan fluorescence intensity. Actin was diluted to 0.1 μM in various buffers containing 10 mM MOPS, 2 mM EDTA, pH 7.0, 20 °C, plus the following additional components: none (○); 2 μM profilin (▽); 100 mM KCl, and 2 μM profilin (□). The upper most curve (◇) shows data for an untreated control of 0.1 μM MgATPactin in 100 mM KCl, 10 mM MOPS, 2 mM $MgCl_2$, 0.2 mM ATP, pH 7.0, 20 °C.

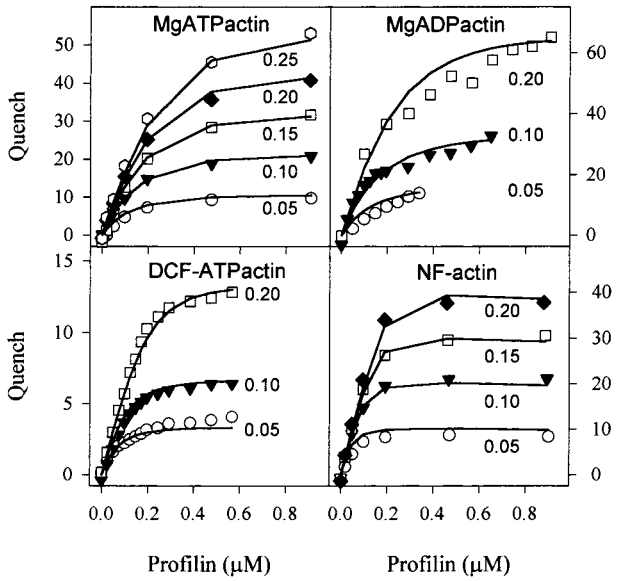

FIGURE 2: Equilibrium profilin binding to β,γ-actin measured by tryptophan fluorescence quenching. Several concentrations of actin (indicated in the figure in μM units) containing bound MgATP, MgADP, ATP, or no bound nucleotide were titrated with profilin. Buffers contained 100 mM KCl, 10 mM MOPS, pH 7.0, 20 °C and: for MgATPactin, 2 mM $MgCl_2$, and 0.2 mM ATP; for MgADPactin, 2 mM $MgCl_2$ and 0.2 mM ADP; for DCF-ATPactin 2 mM EDTA and 1 mM ATP; for NF-actin, 2 mM $MgCl_2$. The denaturation rate of the actin is slow for those experiments containing nucleotide, and NF-actin is stabilized by the presence of 100 mM KCl, and is further attenuated by the addition of profilin during the titrations. Each panel shows data for several concentrations of actin (different symbols represent different initial actin concentrations) and a global fit (lines) to the binding isotherms by a quadratic binding equation. The equilibrium constants for profilin binding to the actin species: MgATPactin, $K_P = 0.099$ ($\pm$0.014) μM; MgADPactin, $K_P = 0.12$ ($\pm$0.05) μM; DCF-ATPactin, $K_P = 0.037$ ($\pm$0.009) μM; NF-actin, $K_P = 0.013$ ($\pm$0.004) μM.

mM ATP (diamonds) shows no change in tryptophan fluorescence, indicating the actin is stabilized by the binding of MgATP. Moreover, because actin polymerization also results in a tryptophan fluorescence quench, potentially complicating the interpretation of this experiment, a constant fluorescence intensity indicates that this low concentration

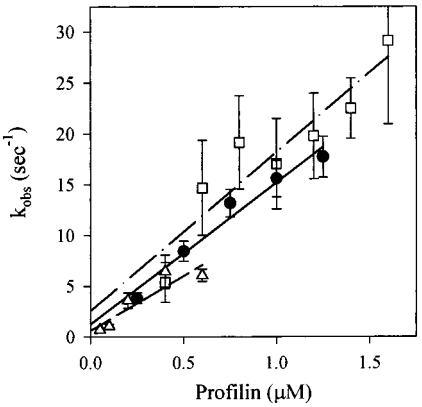

FIGURE 3: Association rate kinetics for profilin binding to β,γ-actin measured by tryptophan fluorescence quenching. Using a stopped-flow reactor, profilin was mixed with MgATPactin, (●, solid line), MgADPactin, (□, dashed−dotted line), or NF-actin, (△, dashed line). Buffers contained 100 mM KCl, 10 mM MOPS, and 2 mM $MgCl_2$, pH 7.0, 20 °C, and additionally for MgATPactin, 0.2 mM ATP, and for MgADPactin, 1 mM ADP. The observed pseudo-first-order rate constants, k_{obs}, for profilin binding to actin were determined from stopped flow measurements of the tryptophan fluorescence quenching time course. Symbols and errors bars represent values and standard errors, respectively, determined from fits to time course data. The association rate constants were determined from linear regression analysis and are 14.0 ($\pm$1.5) μM^{-1} s^{-1}, 15.6 ($\pm$2.9) μM^{-1} s^{-1}, and 10.8 ($\pm$2.7) μM^{-1} s^{-1}, for MgATPactin, MgADPactin, and NF-actin, respectively.

of actin does not polymerize during the time of the experiment, even though the ionic conditions are near optimal for actin polymerization.

These data indicate that profilin binding stabilizes NF-actin and dramatically decreases the rate at which actin irreversibly unfolds. Actin is also stabilized by the presence of 100 mM KCl, a salt concentration which also promotes actin polymerization and causes the actin conformational change as measured by fluorescence of I-AEDANS-labeled actin (*32*). Together, KCl and profilin decrease the rate constant for NF-actin denaturation 40-fold compared to that for NF-actin alone in low ionic strength buffer.

Affinity of Actin for Profilin; Tryptophan Fluorescence Measurements. The affinities of profilin for various isoforms of actin have been measured by indirect techniques which have proven to be problematic. Early measurements used pyrene-labeled actin to monitor changes in the critical concentration of actin. However, profilin has been shown to bind poorly to pyrene-labled actin, complicating this analysis. Furthermore, because the profilin actin complex can add to the barbed ends of filaments, this type of analysis requires addition of a barbed end capping protein. Determination of the affinity of actin for profilin based on the profilin concentration dependence of nucleotide exchange rates can also be misleading as described below (Figure 7). More direct affinity measurements using fluorescence anisotropy of rhodamine-labeled engineered profilin (*4*) and tryptophan fluorescence quenching using only native proteins (*2*) are simpler to interpret.

The affinity of non-muscle β,γ-actin for profilin was determined in the present report by measuring the tryptophan fluorescence intensity quenching that occurs when actin binds profilin (*27*). Figure 2 shows tryptophan fluorescence quench data for profilin titrations of MgATPactin, MgADPactin, DCF-ATPactin, and NF-actin. Each data set of several actin

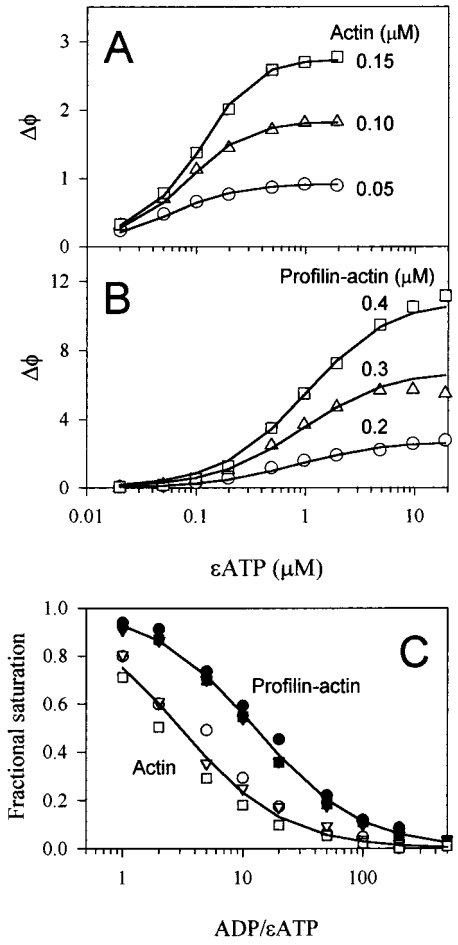

FIGURE 4: Equilibrium binding of nucleotides to β,γ-actin and profilin-β,γ-actin. Experiments were conducted in buffer containing 100 mM KCl, 10 mM MOPS, and 2 mM $MgCl_2$, pH 7.0, 20 °C. (A, B) Various concentrations of NF-actin and profilin-NF-actin, as indicated, were titrated with MgϵATP. The increase in ϵATP fluorescence in the presence of actin above that in the absence of actin, $\Delta\phi$, is plotted versus the ϵATP concentration. Data for three concentrations of actin and a global fit with a quadratic binding equation are shown for each experimental condition. The equilibrium constants for MgϵATP binding to actin and profilin−actin are $K_{Mg\epsilon ATP} = 0.031$ μM (±0.002) and $K^{P}_{Mg\epsilon ATP} = 0.51$ μM (±0.01), respectively. (C) Varying concentrations of ADP were added to 0.2 μM MgϵATPactin (open symbols) or profilin-MgϵATPactin (filled symbols) and the ϵATP fluorescence intensity was converted to fractional saturation with ϵATP. Fits to the data yield the ratio of equilibrium constants for MgADP and MgϵATP binding to actin and profilin−actin, $K_{MgADP}/K_{Mg\epsilon ATP} = 3.0$ (±0.2) and $K^{P}_{MgADP}/K^{P}_{Mg\epsilon ATP} = 12.8$ (±0.4), respectively.

concentrations was globally fit as described in Material and Methods and yielded an equilibrium dissociation constant (K_P) for profilin binding; the values are summarized in Table 1. Profilin binds MgATPactin and MgADPactin with similar affinity, with values for $K_p^T = 0.099$ μM and $K_p^D = 0.12$ μM, respectively. This is in contrast to a previous report using α-skeletal muscle actin that indicated a 20-fold lower affinity of profilin for MgADPactin compared to MgATPactin (*2*). However, the data presented here are in agreement with previously published results from our laboratory using α-skeletal muscle actin that showed similar affinities of profilin for MgATPactin and MgADPactin (*3*). Profilin binds DCF-ATPactin with an equilibrium constant $K_p^{DCF} = 0.037$ μM and binds NF-actin with equilibrium constant $K_p^{NF} =$ 0.013 μM. Thus, removal of Mg^{2+} from the central cleft of MgATPactin increases the affinity for profilin about 3-fold. Removal of MgATP from MgATPactin increases the affinity for profilin by about 8-fold.

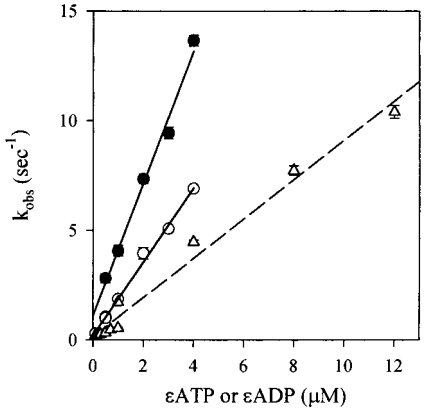

FIGURE 5: Kinetic measurements of the association reaction for binding of nucleotides to β,γ-actin in the absence and presence of profilin. The observed pseudo first-order rate constants, k_{obs}, for MgϵATP or MgϵADP binding to actin and profilin−actin were determined from stopped flow measurements of the fluorescence intensity increases of MgϵATP or MgϵADP upon binding by actin. Values determined for k_{obs} are plotted for NF-actin reacted with MgϵATP (circles) or MgϵADP (△) in the absence (open symbols) or presence (filled symbols) of 2 μM profilin in buffer containing 100 mM KCl, 10 mM MOPS, and 2 mM $MgCl_2$ pH 7.0, 20 °C. Error bars represent standard errors for each k_{obs} value determined from fits to time course data. The rate constants were determined from linear regression analysis of the data sets: k_+ values for MgϵATP binding to actin and profilin−actin are 1.7 (±0.05) μM^{-1} s^{-1} and 3.0 (±0.18) μM^{-1} s^{-1}, respectively; and the k_+ value for MgϵADP binding to actin is 0.9 (±0.04) μM^{-1} s^{-1}.

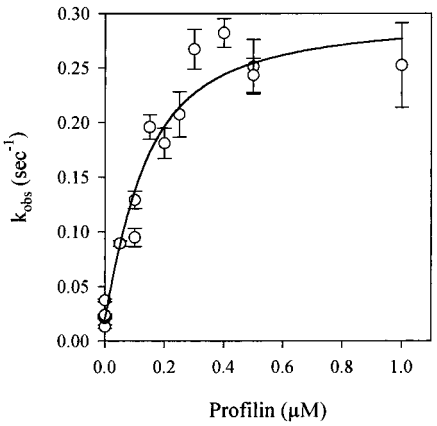

FIGURE 6: Rate constant for MgATP dissociation from β,γ-actin is increased by profilin binding to actin. A stopped flow reactor was used to mix (final concentrations) 0.1 μM MgATPactin with 6 μM ϵATP in buffer containing 100 mM KCl, 10 mM MOPS, 2 mM $MgCl_2$, 0.6 μM ATP, pH 7.0, 20 °C, and various concentrations of profilin. Symbols and errors bars represent k_{obs} values and standard errors, respectively, determined from fits to MgϵATP fluorescence intensity time course data. The data were fit with a quadratic function (see text for details) which yielded the rate constant for dissociation of MgATP from profilin−actin, $k^{P}_{-MgATP} = 0.3$ s^{-1}, and the equilibrium constant for profilin binding to MgATPactin, $K_P = 0.08$ μM.

Kinetic Rate Constants for Profilin Binding to Actin. The association rate constants for profilin binding to actin are useful for modeling the actin-bound nucleotide exchange reaction in the presence of profilin (Figure 7, below), and the kinetic constants can be used to calculate equilibrium

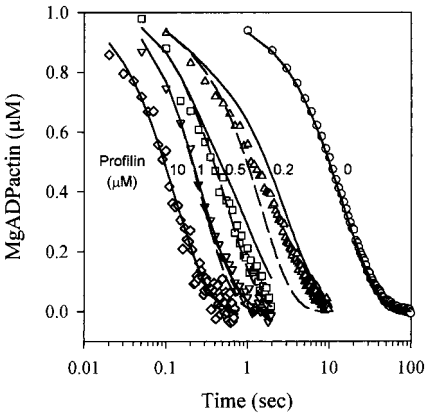

FIGURE 7: Time courses for MgADP dissociation from β,γ-actin in the presence of varying concentrations of profilin. A stopped flow reactor was used to mix 1 μM MgADPactin with MgϵADP and in the presence of (from right to left) 0, 0.2, 0.5, 1, and 10 μM profilin in buffer containing 100 mM KCl, 10 mM MOPS, 2 mM $MgCl_2$, 0.6 μM ATP, pH 7.0, 20 °C. The lines represent a global fit to all six time courses using a series of differential equations as described in the text. The solid lines are calculated with Scheme 1 and with the following values for the rate constants: $k_{-MgADP} = 0.07\ s^{-1}$, $k^P_{-MgADP} = 8\ s^{-1}$, $k_{+p} = 15\ \mu M^{-1}\ s^{-1}$, $k^T_{-p} = 1.5\ s^{-1}$, and $k^D_{-p} = 1.5\ s^{-1}$ (i.e., $K^T_P = K^D_P = 1.5\ s^{-1}/15\ \mu M^{-1}\ s^{-1} = 0.1\ \mu M$). The dashed lines are calculated with the same constants except $k^D_{-p} = 6\ s^{-1}$ (i.e., $K^D_P = k^D_{-p}/k_{+p} = 0.4\ \mu M$).

constants and verify the equilibrium measurements presented in Figure 2. Using a stopped flow reactor, tryptophan fluorescence quenching was measured to determine the rate constants for profilin binding to non-muscle β,γ-actin. Time course data were fit with a single-exponential function to yield values for the observed pseudo-first-order rate constants, k_{obs}. Figure 3 shows the values for k_{obs} as a function of profilin concentration; error bars represent the standard error for each value. Linear regression analysis yielded values for the association rate constant for profilin binding to MgATPactin (circles) $k_{+p} = 14.0\ (\pm 1.5)\ \mu M^{-1}\ s^{-1}$ and dissociation rate constant $k_{-p} = 1.3\ (\pm 1.2)\ s^{-1}$, corresponding values obtained for MgADPactin (squares), $k_{+p} = 15.6\ (\pm 2.9)\ \mu M^{-1}\ s^{-1}$ and $k_{-p} = 2.6\ (\pm 3.1)\ s^{-1}$, and for NF-actin (triangles), $k_{+p} = 10.8\ (\pm 2.7)\ \mu M^{-1}\ s^{-1}$ and $k_{-p} = 0.7\ (\pm 1.2)\ s^{-1}$. The k_{+p} values for MgATPactin, MgADPactin, and NF-actin are not significantly different from each other. The k_{+p} value reported here in buffer containing 100 mM KCl is about 3-fold slower than values previously reported for profilin binding to actin in low ionic strength buffer: for bovine spleen profilin binding to α-skeletal muscle MgATPactin, $k_{+p} = 45\ \mu M^{-1}\ s^{-1}$ (*27*) and for *Acanthamoeba castellanii* profilin binding to *Acanthamoeba castellanii* MgATPactin, $k_{+p} = 35-53\ \mu M^{-1}\ s^{-1}$ (*4*).

Equilibrium Binding of Nucleotides to Actin and Profilin-Actin. Although it is accepted that profilin binding to actin weakens the affinity for nucleotides, the equilibrium constants for nucleotide binding to profilin−actin have not previously been measured directly. Quantitation of the equilibrium constants for nucleotides have been based on nucleotide dissociation rate constants, relative affinities of native and etheno- nucleotides or have been calculated from thermodynamic considerations of an energy square (*2*, *4*, *20*, *33*). The ability to prepare relatively stable NF-actin allows the direct equilibrium measurements of nucleotide binding to profilin−actin using fluorescent nucleotide analogues.

The etheno-nucleotide analogues, ϵATP and ϵADP, increase in fluorescence intensity upon binding to actin. Figure 4, panels A and B, show data from experiments in which aliquots of ϵATP were added to NF-actin; the increase in fluorescence intensity above that in the absence of actin, $\Delta\phi$, is proportional to the amount of bound nucleotide. Fluorescence intensity data for ϵATP in the absence and presence of various concentrations of actin or profilin−actin were globally fit with a quadratic binding equation to yield equilibrium dissociation constants for nucleotide binding to actin. Figure 4 shows $\Delta\phi$ values and fits for titration with ϵATP of various concentrations actin (panel A) and profilin−actin (panel B) yielding respective equilibrium dissociation constants $K_{Mg\epsilon ATP} = 0.031\ (\pm 0.002)\ \mu M$, and $K^P_{Mg\epsilon ATP} = 0.51\ (\pm 0.01)\ \mu M$. A similar experiment (data not shown) using ϵADP titration of actin yielded an equilibrium dissociation constant $K_{Mg\epsilon ADP} = 0.38\ (\pm 0.032)\ \mu M$. However, experiments to measure the affinity of profilin−actin for MgϵADP proved to be inconsistent: the high concentrations of ϵADP needed to saturate the actin, the inner filter effect, and the low signal-to-noise ratio combined to confound the measurements. To more accurately determine the effect of profilin binding on the affinity of actin for ADP, MgϵATP bound to actin and profilin−actin was displaced with varying concentrations of ADP. Panel C shows the results from such experiments in which the fractional saturation of actin or profilin−actin with ϵATP is plotted against the ratio of concentrations of ADP and ϵATP. The data indicate that the ratio of equilibrium constants for actin and nucleotides $K_{MgADP}/K_{Mg\epsilon ATP} = 3.0\ (\pm 0.2)$, and for profilin−actin and nucleotides $K^P_{MgADP}/K^P_{Mg\epsilon ATP} = 12.8\ (\pm 0.4)$. From the relative affinities of MgϵATP and MgADP for actin and profilin−actin (panel C), we can calculate $K_{MgADP} = K_{Mg\epsilon ATP} \times K_{MgADP}/K_{Mg\epsilon ATP} = 0.031\ \mu M \times 3.0 = 0.093\ \mu M$, and $K^P_{MgADP} = K^P_{Mg\epsilon ATP} \times K^P_{MgADP}/K^P_{Mg\epsilon ATP} = 0.51\ \mu M \times 12.8 = 6.5\ \mu M$.

These data indicate that profilin binding by actin differentially affects the relative affinities of actin for MgATP and MgADP. Profilin binding weakens the affinity of actin for both MgATP and MgADP, but weakens MgADP binding 70-fold and weakens MgATP binding 16-fold. Other experiments (data not shown) were conducted in which actin-bound MgϵATP or MgϵADP was displaced with added MgATP or MgADP, respectively. Actin binds MgATP with about 4-fold greater affinity than MgϵATP; similarly, actin binds MgADP with about 4-fold greater affinity than for MgϵADP and the binding of profilin by actin does not alter the ratio of affinities for etheno versus native nucleotides. The 4-fold weaker MgϵATP binding compared to MgATP binding by actin is in good agreement with previously published values for nucleotide binding to α-skeletal actin (*13*, *23*) and in agreement with the dissociation rate constants for native and etheno-nucleotides. Thus, we are able to calculate the equilibrium constants for native nucleotide binding to actin and profilin−actin from the etheno-nucleotide data, and the values are summarized in Table 2.

Kinetics for Nucleotide Association to Actin and Profilin-Actin. Crystal structures of profilin−actin have been solved that exhibit two conformations termed "open" and "tight" states, differing by the relative positions of the two major actin domains that are separated by the central actin cleft

Table 1: Equilibrium and Rate Constants for Profilin Binding to Actin[a]

ligands		K_P (μM)	k_{+p} (μM^{-1} s^{-1})	k_{-p} (s^{-1})	calc. k_{-p} (s^{-1})
NF-actin	profilin	0.013 ± 0.004	10.8 ± 2.7	0.7 ± 0.9	0.14 ± 0.8
DCF-ATPactin	profilin	0.037 ± 0.009			
MgATPactin	profilin	0.099 ± 0.014	14.0 ± 1.5	1.3 ± 1.2	1.4 ± 0.35
MgADPactin	profilin	0.12 ± 0.05	15.6 ± 2.9	2.6 ± 3.1	1.9 ± 1.1

[a] All conditions include 100 mM KCl, 10 mM MOPS, pH 7.0, and either 2 mM $MgCl_2$ or 2 mM EDTA. K_P values were determined from profilin titration experiments (Figure 2) and standard errors are from a fit to the binding isotherms. Values for k_{+p} and k_{-p} were determined from kinetic data (Figure 3) and standard errors are from linear regression to data. Values for calc. k_{-p} were calculated from $K_p k_{+p}$ and standard errors are calculated from the sum of the relative error in each measured value.

Table 2: Equilibrium and Rate Constants for Nucleotide Binding to Actin and Profilin-Actin[a]

ligands		K_D (μM)	$K_D = k_-/k_+$ (μM)	k_- (s^{-1})	k_+ (μM^{-1} s^{-1})
MgADP	actin	0.094[b]	0.079	0.071 ± 0.001	0.90[c]
MgϵADP	actin	0.40 ± 0.02	0.33	0.30 ± 0.01	0.90 ± 0.04
MgATP	actin	0.007[b]	0.0065	0.011 ± 0.003	1.7[c]
MgϵATP	actin	0.031 ± 0.002	0.027	0.046 ± 0.001	1.7 ± 0.1
MgADP	profilin-actin	6.5[b]		8[d]	1.2[e]
MgϵADP	profilin-actin	26[b]		32[d]	1.2[e]
MgATP	profilin-actin	0.13[b]	0.10	0.30 ± 0.03	3.0[c]
MgϵATP	profilin-actin	0.51 ± 0.01	0.38	1.1 ± 0.1	3.0 ± 0.2

[a] Buffers contain 100 mM KCl, 10 mM MOPS, 2 mM $MgCl_2$, pH 7.0, 20 °C. Measured K_D values were determined from data presented in Figure 4, k_- values were determined from exponential fits to time course data, and k_+ values were determined from data presented in Figure 5, except as noted. Measured values include standard errors determined from analysis of experiments. [b] Calculated from the relative affinities of MgϵATP or MgϵADP and MgATP or MgADP, see Figure 4 and text for details. [c] Association rate constants for etheno nucleotides are the same as native nucleotides (*13*). [d] Determined using differential equations model fit to data time courses from Figure 7. [e] Calculated from $k_+ = k_-/K_D$.

(*14*, *16*). These observations suggest that profilin could affect the actin interdomain angle and thereby regulate the affinity of the nucleotide bound in the actin central cleft (*17*); a more open actin cleft could allow faster association and dissociation of nucleotide to profilin−actin. On the basis of data using *Acanthamoeba* proteins, Vinson et al. (*4*) calculated that the k_{+MgATP} value was three times faster for MgATP association to profilin−actin than to actin; in contrast, the binding of profilin to actin slowed the MgADP association rate constant about 2-fold. However, the association rate constant for nucleotide binding to profilin−actin has not been measured directly.

The observed rate constants, k_{obs}, for nucleotide binding to actin were determined by mixing NF-actin with either MgϵATP or MgϵADP in a stopped flow reactor and fitting the time course of the fluorescence intensity increase to an exponential function. The values for k_{obs} are plotted in Figure 5 as a function of MgϵATP (circles) or MgϵADP (triangles) in the absence (open symbols) or presence (filled symbols) of profilin. The rate constant for association of MgϵATP to actin has a value $k_{+Mg\epsilon ATP} = 1.68$ (±0.06) μM^{-1} s^{-1}; the addition of saturating concentration of profilin increases the association rate constant about 2-fold to $k^p_{+Mg\epsilon ATP} = 3.0$ (±0.2) μM^{-1} s^{-1}. The intercept of the linear regression lines with the ordinate indicate an increased value for the rate constant for dissociation of MgϵATP from profilin−actin, qualitatively in agreement with measurements of ATP dissociation rates (see below), but the values have a high uncertainty with about 50% coefficient of variation. The value for the rate constant for association of MgϵADP to actin is $k_{+Mg\epsilon ADP} = 0.90$ (±0.04) μM^{-1} s^{-1} and the value determined from the intercept of the regression line with the ordinate for the MgϵADP dissociation rate constant, $k_{-Mg\epsilon ADP} = 0.15$ (±0.19) s^{-1}. The weak binding of MgϵADP by profilin−actin prevented reliable measurements of the corresponding association rate constant for the same reasons that complicate the equilibrium measurements above; however, $k^p_{+Mg\epsilon ADP}$ can be calculated from $K^p_{Mg\epsilon ADP}$ and $k^p_{-Mg\epsilon ADP}$ (see below) and is listed in Table 2 among the other constants.

Earlier work from our laboratory showed the rate constants for association of MgϵATP and MgATP to actin to be equal (*13*); therefore, in Table 2, we have used the measured association rate constants for the etheno-nucleotide analogues along with measured dissociation rate constants for native nucleotides (see below) to calculate equilibrium constants for binding of MgATP and MgADP to actin and profilin−actin. Our results indicate that binding of profilin by actin increases the association rate constants for MgATP and MgADP, but only to a relatively small extent, less than 2-fold.

Kinetics for MgATP Dissociation from Actin and Profilin-Actin. Measurements of the observed MgATP dissociation rate constant as a function of profilin concentration can be analyzed with a binding function to determine the rate at which MgATP dissociates from profilin−actin, k^p_{-MgATP}, and the equilibrium constant for profilin binding to MgATPactin, K^T_P (see Material and Methods for details). Non-muscle β,γ-MgATPactin was mixed in a stopped flow reactor with varying concentrations of profilin and MgϵATP in a 10-fold molar excess over MgATP concentration. The observed rate constant, k_{obs}, for MgATP dissociation was determined from exponential fits to fluorescence time course data and plotted as a function of profilin concentration (shown in Figure 6). From a fit to the data in Figure 6, the rate constant for MgATP dissociation from actin was determined to be $k_{-MgATP} = 0.02$ (±0.01) and saturation of MgATPactin with profilin increases the MgATP dissociation rate constant to $k^p_{-MgATP} = 0.30$ (±0.02) s^{-1}. The fit to the data also yields an

equilibrium dissociation constant for profilin binding to MgATPactin, $K_P = 0.08$ (± 0.03) μM. Another experiment (not shown) using 1 μM actin yielded values $K_P = 0.16$ (± 0.06) and $k^p_{-MgATP} = 0.35$ (± 0.02) s^{-1}. The values determined for K_P from nucleotide exchange measurements agree well with the value obtained from tryptophan fluorescence intensity measurements, $K_P = 0.1$ μM. The rate constants for dissociation of MgATP from actin and for dissociation of MgϵATP from actin and profilin−actin were measured with additional nucleotide exchange experiments (data not shown) and the values are included in Table 2.

Kinetics for MgADP Dissociation from Actin and Profilin-Actin. It is thought that the enhancement of exchange of actin-bound MgADP for MgATP by profilin may be an important physiological function of profilin, thereby providing a homogeneous pool of MgATPactin that can rapidly add on to the ends of actin filaments during cellular motile events (*20*). Our previous work showed that the rate of MgADP dissociation from monomeric skeletal muscle actin can limit the amount of actin polymer formed in vitro under conditions of high actin filament number concentration approximating that found in vivo (*3*). The quantitation of actin bound MgADP exchange using non muscle β,γ-actin under physiological ionic conditions should provide information useful for modeling intracellular motile systems.

To determine the effect of profilin on MgADP dissociation, MgADPactin was mixed in a stopped flow reactor with a MgϵATP concentration in excess of the MgADP concentration; the observed rate of nucleotide exchange is limited by the dissociation of MgADP from actin. Figure 7 shows nucleotide exchange time course data for 1 μM MgADPactin. The analysis used for MgATP dissociation from actin in the presence of profilin (Figure 6) is not valid for the case of MgADP dissociation from actin because MgADP dissociates from profilin−actin rapidly relative to the kinetics of profilin interaction with actin. The time to equilibrium for profilin binding to actin is $\tau = 1/(k_{+p}[\text{profilin}] + k_{-p})$, where $k_{+p} = 15$ μM^{-1} s^{-1} and $k_{-P} = 1.5$ s^{-1}; therefore, we can calculate a value for the time constant for 0.5 μM profilin, $\tau \approx 0.1$ s. From Figure 7, the exchange of MgADP for MgϵATP in the presence of 0.5 μM profilin has a half time of about 0.03 s; therefore, profilin cannot be considered in rapid pre-equilibrium with MgADPactin. The nucleotide exchange reaction in the presence of profilin can be described by Scheme 1, from which we can derive the following series of differential equations:

$$\frac{d[AD]}{dt} = -k_{+p}[P][AD] + k^D_{-p}[PAD] - k_{-MgADP}[AD]$$

$$\frac{d[AT]}{dt} = -k_{+p}[P][AT] + k^T_{-p}[PAT] + k_{-MgADP}[AD]$$

$$\frac{d[PAD]}{dt} = k_{+p}[P][AD] - k^D_{-p}[PAD] - k^p_{-MgADP}[PAD]$$

$$\frac{d[PAT]}{dt} = k_{+p}[P][AT] - k^T_{-p}[PAT] + k^p_{-MgADP}[PAD]$$

where AD and AT are actin containing bound MgADP and MgϵATP, respectively; PAD and PAT are profilin−actin complexes containing bound MgADP and MgϵATP, respectively; P is profilin; k_{-MgADP} and k^p_{-MgADP} are the rate constants for MgADP dissociation from actin and profilin−actin, respectively; k_{+p} is the association rate constant for profilin and actin; k^D_{-p} and k^T_{-p} are the respective rate constants for profilin dissociation from MgADPactin or MgϵATPactin. From mass conservation,

Scheme 1

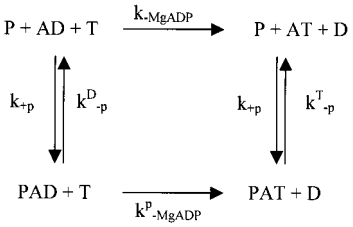

$$[P] = [P_{tot}] - [PAT] - [PAD]$$

$$[AT_{tot}] = [AT] + [PAT]$$

where [P] is free profilin and $[AT_{tot}]$ is the total MgϵATPactin concentration.

The fluorescence data were converted to MgϵATPactin concentrations as shown in Figure 7, and the predetermined values for $k_{-MgADP} = 0.07$ s^{-1}, $k_{+p} = 15$ μM^{-1} s^{-1}, $k^D_{-p} = 1.5$ s^{-1}, and $k^T_{-p} = 1.5$ s^{-1} were used to calculate the solid lines. The single parameter k^p_{-MgADP} was varied manually to achieve a best fit to the nucleotide exchange time course data, and a value $k^p_{-MgADP} = 8$ s^{-1} was determined. To test the possibility that profilin binds weaker to MgADPactin than MgATPactin, the dashed lines show time courses calculated using the same constant as above except for $k^D_{-p} = 6$ s^{-1} ($K^D_P = k^D_{-p}/k_{+p} = 0.4$ μM). The time course data are fit by the model about equally well using the two values for K_P which are different by a factor of 4; therefore, from these data we cannot rule out a differential affinity of profilin for MgADPactin and MgATPactin.

Effect of Profilin on Dissociation of ATP from DCF-ATPactin. The dissociation rate of nucleotides from actin has been shown to be limited by the dissociation of the high affinity divalent cation and to be dependent on the concentration of divalent cations in solution (*13*). Removal of the high affinity divalent cation from actin reduces the affinity of actin for nucleotide by orders of magnitude (*13*). Because profilin binding by actin also weakens the affinity of actin for nucleotides, it is of interest to examine the effect of profilin binding by DCF-ATPactin. Figure 8 shows the time course data for nucleotide exchange experiments in which ϵATP binding to DCF-actin is limited by the dissociation of ATP from DCF-ATPactin. The dissociation time courses are shown for DCF-ATPactin in the absence (upper panel) and presence (lower panel) of profilin. The data (symbols) were fit with an exponential function (lines) to yield values for the dissociation rate constant of ATP from actin $k_{-ATP} = 39.4$ (± 4.7) s^{-1}. Addition of a saturating amount of profilin results in about a 40% faster ATP dissociation rate constant $k^P_{-ATP} = 55.7$ (± 6.5) s^{-1}. Actin conformational changes caused by profilin binding to DCF-ATPactin apparently do little to accelerate nucleotide dissociation compared to the approximately 30-fold enhancement of MgATP dissociation and 100-fold enhancement of MgADP dissociation. It must

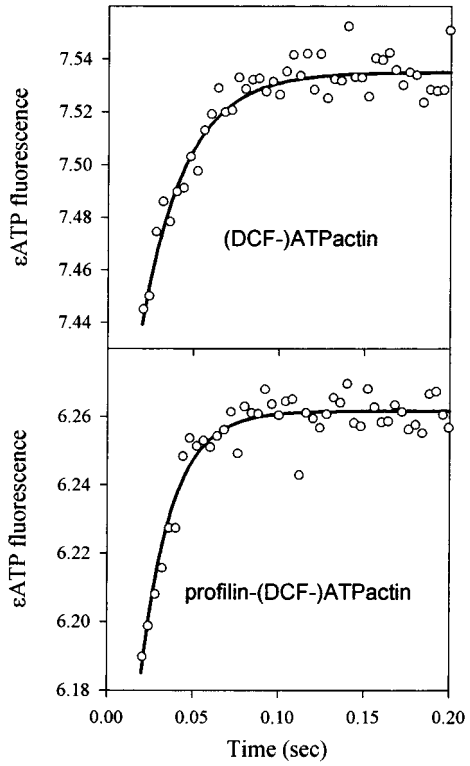

FIGURE 8: Time courses for ATP dissociation from β,γ-DCF-ATPactin in the absence and presence profilin. CaATPactin was diluted into buffer containing 10 mM MOPS, 2 mM EDTA, pH 7.0, to remove the tightly bound Ca^{2+} ion, then mixed with ϵATP in a stopped-flow reactor to yield final concentrations of 125 μM ϵATP, 25 μM ATP, 2.5 μM DCF-ATPactin, and either 3 μM profilin or no profilin. The lines are exponential fits to the data and yield the rate constants for dissociation of ATP from DCF-ATPactin, $k_{-ATP} = 39.4\ (\pm 4.7)\ s^{-1}$, and from profilin-DCF-ATPactin, $k^{p}_{-ATP} = 55.7\ (\pm 6.5)\ s^{-1}$.

be that disruption of Mg^{2+} coordination in the nucleotide binding cleft of actin is the predominant mechanism by which profilin enhances nucleotide dissociation from actin.

DISCUSSION

Comparison of Actin Isoforms. To better understand the role of profilin in cellular motile processes that involve actin polymerization, we have characterized the interaction of profilin with non-muscle β,γ-actin. Although some studies with non-muscle actin isotypes have been reported, the physiological MgATP- and MgADP-containing forms of vertebrate non-muscle β,γ-actin in the presence of physiological salt concentrations have not been characterized. X-ray crystallographic structures of profilin-β-actin (*16*) show differences from both the α-actin-DNase I structure (*34*) and the α-actin-gelsolin segment 1 structure (*35*), but there are no direct crystallographic structure comparisons of the actin isoforms either alone or complexed with the same actin-binding protein. Comparison of the work presented here with our previously published data for α-skeletal muscle actin (*3*, *13*) shows some functional differences between the muscle and non-muscle actin isoforms. Profilin binds to non-muscle actin with about 6-fold greater affinity than to α-skeletal muscle actin. Nonmuscle actin exchanges its bound MgADP for MgATP about 7-fold faster than does muscle actin (*3*). Of particular interest is the enhanced nucleotide exchange reaction that occurs when profilin binds MgADPactin. Under physiological ionic conditions, non-muscle MgADPactin complexed with profilin exchanges nucleotide with a rate constant of 8 s^{-1}, about 6-fold faster than does α-skeletal muscle profilin−actin. Another striking difference between α-actin and β,γ-actin isoforms is the denaturation rate of NF-actin; α-skeletal muscle NF-actin denatures 15-fold faster than does non-muscle β,γ-NF-actin.

Actin Denaturation. Actin denaturation proceeds through the labile intermediate species NF-actin (*13*, *36*). The lessened stability of NF-actin suggests that the loss of interdomain coupling that occurs when the nucleotide is removed leads to irreversible unfolding. Conformational changes have been shown to take place in actin through a shear motion involving an alpha helix at the bottom of the actin interdomain cleft that links subdomains 1 and 3 and allows the two domains to rotate relative to one another (*14*, *15*). Data from denaturation experiments support the idea that profilin binding between actin subdomains 1 and 3 at the "barbed" end of the actin molecule may provide alternative actin interdomain coupling thereby stabilizing NF-actin against unfolding (*37*).

In low ionic strength buffer, α-skeletal muscle NF-actin denatures rapidly with $\tau_{den} = 5$ s (*13*), reflecting a denaturation rate about 15-fold faster than that for non-muscle β,γ-NF-actin as reported here. This observation appears to contradict the conclusion drawn by Schuler et al. (*36*), who reported that the α-actin isoform was more stabile than non-muscle β,γ-actin isoforms. They also reported that profilin decreased the stability of actin containing bound MgATP or CaATP, whereas, in contrast, we find that profilin greatly stabilizes NF-actin. However, in their experiments the denaturation of actin was monitored in the presence of MgATP or CaATP, and thus, the observed denaturation rate was limited by the rate of NF-actin formation (i.e., the dissociation rate of nucleotide from actin), which is faster for non-muscle actin than for muscle actin and is increased by profilin.

Actin Tryptophan Fluorescence Quenching by Profilin Binding. The well documented tryptophan fluorescence quenching that occurs upon binding of profilin to actin suggests that profilin binding alters the conformation of actin. Perelroizen et al. (*27*) concluded that profilin binding by actin resulted in quenching of actin tryptophan residues and that the solvent accessible actin tryptophans are no longer exposed to the solvent in the profilin−actin complex. The four tryptophans of actin are located in subdomain 1 which has direct contact with profilin; therefore, tryptophan fluorescence alone does not reveal how profilin changes the conformation of other more distal portions of the actin molecule.

Data from titrations of β,γ-actin with profilin presented here indicate that profilin binds to MgATPactin and MgADPactin with similar affinity. This finding is in agreement with reports for α-skeletal muscle actin that also used actin tryptophan fluorescence to measure profilin binding (*4*, *27*). Our nucleotide exchange experiments (Figures 6 and 7) are also consistent with equal affinity of profilin for MgATPactin and MgADPactin although they do not rule out differential affinity of profilin for MgATPactin and MgADPactin. Vinson et al. reported about a 4-fold greater affinity of profilin for MgATPactin compared to MgADPactin for both α-actin and amoeba actin using

tryptophan quenching for amoeba actin and using fluorescence anisotropy of labeled profilin for both muscle actin and amoeba actin (*4*). We cannot explain these discrepancies between methods for measuring profilin affinity for actin.

Profilin Regulation of Nucleotide Exchange on Actin. Measurements of nucleotide exchange on non-muscle β,γ-actin indicate that profilin increases the MgATP dissociation rate constant value about 30-fold to a maximal value of $k^{P}_{-MgATP} = 0.3\ s^{-1}$. This magnitude of enhancement of MgATP dissociation by profilin is comparable to that previously reported for α-skeletal muscle MgATPactin of 32-fold (*3*) and 40-fold (*2*). Profilin was found to increase the MgADP dissociation rate constant 114-fold to $k^{P}_{-MgADP} = 8\ s^{-1}$, similar to the 160-fold increase (*3*) and 120-fold increase (*2*) reported for α-skeletal muscle MgADPactin. The value for the equilibrium dissociation constant for profilin binding to MgATPactin derived from nucleotide exchange experiments (Figure 6), $K^{T}_{P} = 0.08\ \mu M$, agrees with the K_P value determined from fluorescence quenching titrations (Figure 2), $K^{T}_{P} = 0.1\ \mu M$. Because the rate constant for MgADP dissociation from β,γ-actin is relatively fast compared to profilin binding, a simple analysis of the observed MgADP dissociation rate constants which assumes a rapid profilin pre-equilibrium for nucleotide exchange is not valid. We demonstrate that the time course for MgADP dissociation from β,γ-actin is described by a 114-fold increase in the MgADP dissociation rate constant upon profilin binding by actin and an equilibrium dissociation constant for profilin binding to MgADPactin similar to that for binding to MgATPactin, in the range 0.1−0.4 μM. This is in contrast to what had been reported assuming a simple hyperbolic dependence of MgADP exchange rate constants on profilin concentration, from which it was concluded that profilin binds to MgADPactin with 20-fold lower affinity than to MgATPactin (*2*).

Nucleotide Binding Kinetics. Profilin-actin has been shown by X-ray crystallography to exist in two conformationally distinct states termed "open" and "tight" (*14*, *16*). In the tight state the nucleotide appears to be sterically blocked from dissociating from actin and has little solvent accessible area (1.8 Å^2). This tight structure is very similar to the DNase I-actin structure which is known to release nucleotide very slowly (*34*). In contrast, the open profilin−actin structure has a greater interdomain separation, and the nucleotide has a much greater solvent accessible area (52.5 Å^2) (*14*). It would appear that in order for nucleotide to either enter or leave the binding site in the central actin cleft, the actin conformation would have to resemble that of the open profilin−actin structure. Closing of the actin interdomain cleft and steric blockage of the nucleotide release may in part be responsible for the very high affinity of actin for nucleotides.

Measurements of the kinetics of binding of MgATP and MgADP to actin and profilin−actin support the idea that profilin binding to actin either opens the actin interdomain cleft or shifts the conformational equilibrium toward the open state (*4*). Such a conformational shift would relax the steric constraints to nucleotide dissociation and result in a much higher dissociation rate constant; similarly, a more open target for nucleotide association could increase the association rate constant. We find that the rate constants for association of MgATP and MgADP to actin are increased less than 2-fold when profilin binds actin. Asymmetrical effects on association and dissociation reactions result in an overall weakening of equilibrium affinity for MgADP and MgATP to profilin−actin compared to actin alone, and suggest that more than steric factors are responsible for the profilin-induced change in affinity of actin for nucleotides.

Scheme 2

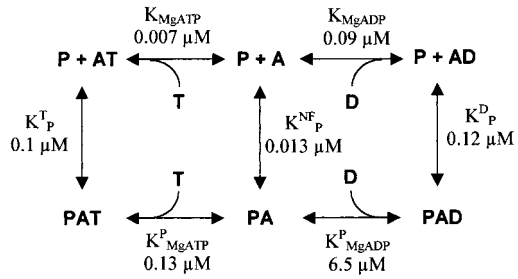

Equilibrium Binding of Profilin and Nucleotides to Actin. Scheme 2 illustrates the equilibrium reactions involved in nucleotide and profilin binding to actin. A and P represent actin and profilin, respectively, T and D represent MgATP and MgADP, respectively, and PA, PAT, and PAD represent the complexes of profilin with NF-actin, MgATPactin, and MgADP actin, respectively. In Scheme 2, two energy squares are linked by the central reaction of profilin binding to NF-actin: P + A ↔ PA. From thermodynamic considerations, the equilibrium constants calculated between states must be independent of the paths taken, and the products of the equilibrium constants around each square must be equal to 1. For the MgATPactin cycle, starting with P + A, and going counterclockwise, 0.007 μM × 0.1 μM × (0.13 μm × 0.013 μM)$^{-1}$ = 0.54. For the MgADPactin cycle, starting with P + A and going clockwise, 0.09 × 0.12 μM × (6.5 × 0.013 μM)$^{-1}$ = 0.13. The product of measured equilibrium constants differ from the theoretical product of 1, by about a factor of 2 for the ATP cycle and by about a factor of 8 for the ADP cycle. The sum of the relative standard errors for the equilibrium constants for the MgATP-actin-profilin square is 90% and for the MgADP-actin-profilin square is 120%. Thus, the equilibrium constants for the ATP energy square are consistent considering the size of the cumulative estimated error going around the square. In contrast, the ADP energy square does not appear consistent.

To explain the apparently inconsistent energetics, we can consider that either the scheme is incorrect or one or more of the constants are inaccurate. Since the MgATP energy cycle is consistent, it appears that the scheme itself is correct. Although we have measured the binding of profilin to actin containing various bound nucleotides with both equilibrium and kinetic experiments, the relatively low signal-to-noise ratio of the tryptophan fluorescence signal and the sensitivity of the fluorescence signal to factors such as protein denaturation and aggregation can complicate such measurements. The constants for nucleotide binding to actin and profilin−actin have been verified by correlation between kinetic and equilibrium measurements with the exception of MgADP binding to profilin−actin, which was determined from different methodology using competitive equilibrium binding experiments. The data (Figure 4) clearly show that profilin binding changes the relative affinity of non-muscle β,γ-actin for MgATP versus MgADP in agreement with what was reported for skeletal muscle α-actin (*3*). Starting with the

ratio of the nucleotide equilibrium dissociation constants for the bottom and top sides of the energy squares in Scheme 2, $K^{P}_{ATP}/K_{ATP} = 19$ and $K^{P}_{MgADP}/K_{MgADP} = 72$, we can calculate the preference of profilin−actin for MgATP over MgADP is 72/19 = 3.8-fold greater than that for actin. Using these numbers and the relationships from Scheme 2, $K^{P}_{MgATP}/K_{MgATP} = K^{T}_{P}/K^{NF}_{P}$ and $K^{P}_{MgADP}/K_{MgADP} = K^{D}_{P}/K^{NF}_{P}$, we can calculate $K^{D}_{P}/K^{T}_{P} \approx 3.8$; therefore, profilin should bind MgADPactin 3.8-fold more weakly than MgATPactin. This calculation argues that the imbalance in the MgADPactin cycle could be due to overestimation of the affinity of profilin for MgADPactin. It has been reported by others (*4*) that profilin binds MgADPactin with ∼4-fold weaker affinity, as discussed above. If K^{P}_{MgADP} were 4-fold greater, (i.e., 0.48 μM), the product of the constants around the energy square would then equal about 0.5 and would then appear to be energetically consistent. If that were the case, then the products for the MgATP and MgADP energy cycles would both equal 0.5, and it would suggest that the affinity for profilin for NF-actin is 2-fold greater than the 0.013 μM value determined here (i.e., 0.0065 μM).

Equilibrium measurements of nucleotide affinity show that non-muscle β,γ-actin binds MgATP with 13-fold greater affinity than MgADP. This preference for MgATP is further enhanced upon profilin binding to actin; profilin−actin binds MgATP with 50-fold greater affinity than MgADP. This enhanced preference of profilin−actin for MgATP over MgADP was also reported for α-skeletal muscle actin (*3*). How does profilin differentially affect MgATP versus MgADP binding to actin? Scheme 2 does not explicitly consider the equilibria of Mg^{2+} binding to ATP and ADP; ATP binds Mg^{2+} with 20−30-fold greater affinity than does ADP (*13*, *25*). If we consider that actin undergoes transient opening and closing movements of the central cleft, profilin binding to actin may affect the actin conformational equilibrium. If Mg^{2+} coordination in the actin nucleotide binding cleft is transiently disrupted by such actin conformational dynamics, then the ability of the bound nucleotide to retain a bound Mg^{2+} during a transient conformational shift may contribute to the observed lifetime of the nucleotide in the cleft. Given the much weaker affinity for Mg^{2+} of ADP than ATP, Mg^{2+} bound to ADP in the actin cleft might dissociate within the lifetime of the open state, resulting in DCF-ADPactin to which ADP is weakly bound. Comparison with MgATPactin suggests that Mg^{2+} bound to ATP in the actin cleft would be much less likely to dissociate within the lifetime of the open state and more likely to reform ligation bonds with the protein so that the high affinity MgATP complex would be retained in the cleft.

Role of Mg^{2+} in Maintaining Actin Structure. ATP and ADP binding to actin have been shown to be mediated by divalent cation binding to the nucleotide phosphates and protein amide groups (*13*, *16*, *34*). The mechanism established for divalent cation and nucleotide exchange on actin is not changed by binding of profilin to actin (*2*). The recently published structure of *Dictyostelium* actin complexed with gelsolin segment 1 (*38*) includes water molecules that are shown to participate in the pentagonal bipyramid coordination of the bound Ca^{2+} in addition to the coordination by the O2β and O2γ phosphate oxygens of ATP; these water molecules also form hydrogen bonds with the δ1 and δ2 oxygens of Asp11, the δ1 oxygen of Asp154, and the ϵ1 oxygen of Gln137 of actin, illustrated in Figure 9. Other actin structures lacking water molecules suggest the same coordination for the high affinity divalent cation by ATP phosphate oxygens and actin residues Asp11, Gln137, and Asp154 (*16*, *34*, *35*). A structure for the physiologic form of actin containing Mg^{2+} bound at the high affinity site is not available; in contrast to what has been found for Ca^{2+}, the Mg^{2+} ion may be expected to be bound with an octahedral coordination sphere that is typically found in MgATPases and MgGTPases (*39*−*41*).

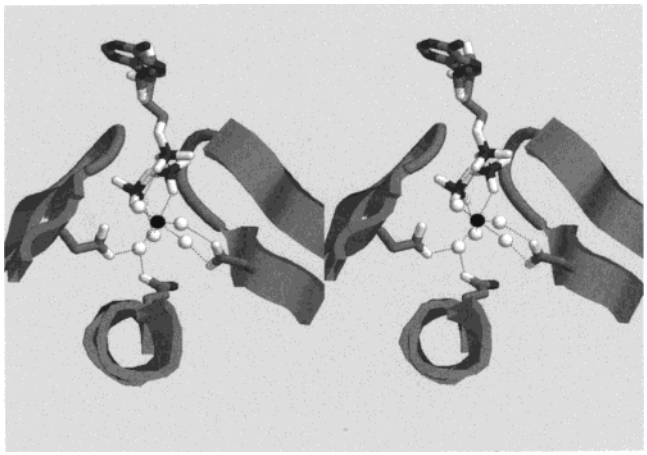

FIGURE 9: Stereoview illustrating the role of the tightly bound divalent cation in actin interdomain coupling. Segments of the phosphate binding loops and the interdomain helix of actin are shown as ribbon representations, ATP, Asp11, Gln137, and Asp154 are shown as stick representations, Ca^{2+} and waters are shown as balls, and the Ca^{2+} ligation and hydrogen bonds are shown as dashed lines. The shades of gray depict the following atoms: white, oxygen; gray, carbon; dark gray, nitrogen and phosphorus; black, calcium. Taken from the structure of *Dictyostelium*/*Tetrahymena* half chimera-1 actin (*38*) (PDB accession code 1C0G) and drawn with RasMol (Windows Version 2.7.1).

In addition to intramolecular salt bridges and the protein interactions with bound nucleotide that provide interdomain coupling in actin, the water mediated coordination of the high affinity divalent cation links actin subdomains 1 (Asp11) and 3 (Asp154) and the interdomain helix 135−150 (Gln137) (*14*, *16*, *38*). Figure 9 illustrates a partial view of CaATPactin centered around the high affinity divalent cation showing a ribbon drawing of three segments of the protein backbone. Shown on the right of Figure 9 is segment 10−19 from the subdomain 1 phosphate binding loop, on the left is segment 153−161 from the subdomain 3 phosphate binding loop, and at the bottom of the figure is segment 137−144 from the interdomain helix. The transition between the tight and open actin states takes place through shear motions involving rotations of Gln137, Ala138, Leu140, Leu142, and Arg335 (*15*). Since Gln137 is part of the interdomain helix that enables actin domain movements and Gln137 also coordinates the high affinity divalent cation—via hydrogen bonds with an intervening water molecule—this residue provides a link between the high affinity divalent cation and actin domain motions. It is interesting to note that the ATP dissociation rate constant from DCF-ATPactin is only slightly affected by profilin binding to actin. Profilin may weaken nucleotide binding by interfering with divalent cation coordination by Asp11, Gln137, and Asp154. A similar mechanism has been proposed to explain how guanine

nucleotide exchange factors (GEF) activate GTPases; the binding of GEF by a GTPase disrupts the Mg^{2+} coordination at the GTP binding site resulting in rapid nucleotide dissociation, and GEF binding stabilizes the nucleotide-free GTPase (*42*). The open state structure of profilin-CaATPactin (*14*) shows that the Ca^{2+} ion interacts only with the ATP phosphate oxygens; this disruption of the divalent cation coordination by protein residues would be expected to greatly weaken the observed binding of the nucleotide to profilin−actin. A reciprocal effect is that the absence of divalent cation in the actin central cleft affects the profilin binding to actin, increasing the affinity severalfold.

It appears that the Mg^{2+} and profilin are pulling on opposite sides of the hinge between the two major actin domains, exerting opposing forces on the structure. By analogy, one could envision the actin molecule as a clothes pin with MgATP pinched by the spring tension in the clamping end of the clothespin. Profilin pulls on the handle end of the clothespin opening it and releasing the MgATP from the clamp. Extending the analogy, with profilin inserted between the two lever arms of the clothes pin handle, the open clamping end is prevented from opening too far against the spring tension; this prevents breaking the spring which would result in a nonfunctional (denatured) clothespin.

CONCLUSIONS

The data in the present report support the idea that profilin opens the central cleft of actin to some degree but restricts further opening (*37*). Profilin binding to NF-actin slows down the irreversible unfolding that results in actin denaturation, suggesting that the actin interdomain coupling which is lost when nucleotide and divalent cation are absent is compensated for by the actin interdomain coupling via profilin. This seems plausible considering that profilin contacts both subdomains 1 and 3 of actin (*16*) and that actin subdomains 3 and 4 do not move independently of each other but function as a single conformational unit (*15*). Profilin binding to actin increases both the association and dissociation rate constants for nucleotide binding to actin, implying that the interdomain cleft of actin becomes more open. Compared to those for actin, the MgATP and MgADP association rate constants for profilin−actin are less than 2-fold faster, but the rate constants for MgATP and MgADP dissociation from profilin−actin are 30-fold and 114-fold faster, respectively. Moreover, the ATP dissociation rate constant from DCF-ATPactin is only slightly accelerated by profilin binding. Apparently, the principal mechanism by which profilin affects nucleotide binding to actin is via disruption of the divalent metal coordination in the actin nucleotide binding cleft. Analogous to what has been suggested for GEF activation of GTPases (*42*), profilin may act as an adenine exchange factor.

NOTE ADDED IN PROOF

Structures are now available in the Protein Data Bank for MgATPactin complexed with gelsolin segment 1: PDB ID's 1DGA, 1YAG, and 1YVN. They all show octahedral coordination of the bound Mg^{2+}.

ACKNOWLEDGMENT

We thank Enrique De La Cruz for helpful discussions on the preparation of NF-actin and determination of the constants involved in Scheme 2. We also thank Willie Wriggers for the shading scheme used in Figure 9.

REFERENCES

1. Schluter, K., Jockusch, B. M., and Rothkegel, M. (1997) *Biochim. Biophys. Acta 1359*, 97−109.
2. Perelroizen, I., Carlier, M. F., and Pantaloni, D. (1995) *J. Biol. Chem. 270*, 1501−1508.
3. Selden, L. A., Kinosian, H. J., Estes, J. E., and Gershman, L. C. (1999) *Biochemistry 38*, 2769−2778.
4. Vinson, V. K., De La Cruz, E. M., Higgs, H. N., and Pollard, T. D. (1998) *Biochemistry 37*, 10871−10880.
5. Korenbaum, E., Nordberg, P., Bjorkrgren-Sjogren, C., Schutt, C. E., Lindberg, U., and Karlsson, R. (1998) *Biochemistry 37*, 9274−9283.
6. Theriot, J. A., and Mitchison, T. J. (1993) *Cell 75*, 835−838.
7. Pantaloni, D., and Carlier, M. F. (1993) *Cell 75*, 1007−1014.
8. Blanchoin, L., Amann, K. J., Higgs, H. N., Marchand, J. B., Kaiser, D. A., and Pollard, T. D. (2000) *Nature 404*, 1007−1011.
9. Finkel, T., Theriot, J. A., Dise, K. R., Tomaselli, G. F., and Goldschmidt-Clermont, P. J. (1994) *Proc. Natl. Acad. Sci. U.S.A. 91*, 1510−1514.
10. McGough, A., Pope, B., Chui, W., and Weeds, A. (1997) *J. Cell Biol. 138*, 771−781.
11. Carlier, M. F., Laurent, V., Santolini, J., Melki, R., Didry, D., Xia, G. X., Hong, Y., Chua, N. H., and Pantaloni, D. (1997) *J. Cell Biol. 136*, 1307−1322.
12. Perelroizen, I., Didry, D., Christensen, H., Chua, N. H., and Carlier, M. F. (1996) *J. Biol. Chem. 271*, 12302−12309.
13. Kinosian, H. J., Selden, L. A., Estes, J. E., and Gershman, L. C. (1993) *J. Biol. Chem. 268*, 8683−8691.
14. Chik, J. K., Lindberg, U., and Schutt, C. E. (1996) *J. Mol. Biol. 263*, 607−623.
15. Page, R., Lindberg, U., and Schutt, C. E. (1998) *J. Mol. Biol. 280*, 463−474.
16. Schutt, C. E., Myslik, J. C., Rozycki, M. D., Goonesekere, N. C. W., and Lindberg, U. (1993) *Nature 365*, 810−816.
17. Rozycki, M. D., Myslik, J. C., Schutt, C. E., and Lindberg, U. (1994) *Curr. Opin. Cell Biol. 6*, 87−95.
18. Selden, L. A., Kinosian, H. J., Estes, J. E., and Gershman, L. C. (2000) *Biochemistry 39*, 64−74.
19. Lindberg, U., Schutt, C. E., Hellsten, E., Tjader, A.-C., and Hult, T. (1988) *Biochim. Biophys. Acta 967*, 391−400.
20. Goldschmidt-Clermont, P. J., Machesky, L. M., Doberstein, S. K., and Pollard, T. D. (1991) *J. Cell Biol. 113*, 1081−1089.
21. Kaiser, D. A., Goldschmidt-Clermont, P. J., Levine, B. A., and Pollard, T. D. (1989) *Cell Motil Cytoskeleton 14*, 251−262.
22. Gershman, L. C., Selden, L. A., Kinosian, H. J., and Estes, J. E. (1989) *Biochim. Biophys. Acta. 995*, 109−115.
23. De La Cruz, E. M., and Pollard, T. D. (1995) *Biochemistry 34*, 5452−5461.
24. De La Cruz, E. M., Mandinova, A., Steinmetz, M. O., Stoffler, D., Aebi, U., and Pollard, T. D. (2000) *J. Mol. Biol. 295*, 517−526.
25. Dawson, R. M. C., Elliott, D. C., Elliot, W. H., and Jones, K. M. (1969) *Data for Biochemical Research*, 2nd ed., Oxford University Press, New York.
26. Weast, R. C. (1968) *CRC Handbook of Chemistry and Physics*, 49 ed., The Chemical Rubber Company, Cleveland.
27. Perelroizen, I., Marchand, J. B., Blanchoin, L., Didry, D., and Carlier, M. F. (1994) *Biochemistry 33*, 8472−8478.
28. Bertazzon, A., Tian, G. H., Lamblin, A., and Tsong, T. Y. (1990) *Biochemistry 29*, 291−298.
29. Lehrer, S. S., and Kerwar, G. (1972) *Biochemistry 11*, 1211−1217.
30. Kuznetsova, I. M., Biktashev, A. G., Khaitlina, S. Y., Vassilenko, K. S., Turoverov, K. K., and Uversky, V. N. (1999) *Biophys. J. 77*, 2788−2800.

31. Turoverov, K. K., Biktashev, A. G., Khaitlina, S. Y., and Kuznetsova, I. M. (1999) *Biochemistry 38*, 6261−6269.
32. Selden, L. A., Estes, J. E., and Gershman, L. C. (1989) *J. Biol. Chem. 264*, 9271−9277.
33. Vinson, V. K., Archer, S. J., Lattman, E. E., Pollard, T. D., and Torchia, D. A. (1993) *J. Cell Biol. 122*, 1277−1283.
34. Kabsch, W., Mannherz, H. G., Suck, D., Pai, E. F., and Holmes, K. C. (1990) *Nature 347*, 37−44.
35. McLaughlin, P. J., Gooch, J. T., Mannherz, H. G., and Weeds, A. G. (1993) *Nature 364*, 685−692.
36. Schuler, H., Lindberg, U., Schutt, C. E., and Karlsson, R. K. (2000) *Eur. J. Biochem. 267*, 476−486.
37. Schuler, H., Korenbaum, E., Schutt, C. E., Lindberg, U., and Karlsson, R. (1999) *Eur. J. Biochem 265*, 210−220.
38. Matsuura, Y., Stewart, M., Kawamoto, M., Kamiya, N., Saeki, K., Yasunaga, T., and Wakabayashi, T. (2000) *J. Mol. Biol. 296*, 579−595.
39. Scheffzek, K., Klebe, C., Fritz-Wolf, K., Kabsch, W., and Wittinghofer, A. (1995) *Nature 374*, 378−381.
40. Fisher, A. J., Smith, C. A., Thoden, J. B., Smith, R., Sutoh, K., Holden, H. M., and Rayment, I. (1995) *Biochemistry 34*, 8960−8972.
41. Weber, J., Hammond, S. T., Wilke-Mounts, S., and Senior, A. E. (1998) *Biochemistry 37*, 608−614.
42. Pan, J. Y., and Wessling-Resnick, M. (1998) *Bioessays 20*, 516−521.

BI001520+